ELSEVIER

Neutron diffraction study and magnetotransport properties of stoichiometric CaMoO₃ perovskite prepared by a soft-chemistry route

C. de la Calle[a],*, J.A. Alonso[a], M. García-Hernández[a], V. Pomjakushin[b]

[a]*Instituto de Ciencia de Materiales de Madrid, CSIC, Cantoblanco, 28049 Madrid, Spain*
[b]*Laboratory for Neutron Scattering, ETHZ & PSI, CH-5232 Villigen PSI, Switzerland*

Abstract

Polycrystalline CaMoO₃ perovskite has been prepared by soft-chemistry procedures, followed by controlled annealing under reducing conditions (H_2/N_2 flow). The crystal structure, studied from neutron powder diffraction data, can be described in an orthorhombic unit cell, space group *Pbnm* (No. 62). The lattice parameters were $a = 5.4510(1)$ Å, $b = 5.5821(1)$ Å and $c = 7.7803(2)$ Å. In the perovskite network the MoO_6 octahedra are tilted by $13.5°$ in order to optimize the Ca–O bond lengths; the tilting scheme corresponds to a GdFeO₃-like superstructure. The perovskite is fully oxygen stoichiometric, as demonstrated from the refinement of the oxygen occupancy factors. Resistivity and transport measurements indicated that CaMoO₃ behaves as a metal; at low temperatures (5 K) a small positive magnetoresistance is observed, reaching a maximum value of 1.4% at 9 T. The magnetic susceptibility is predominantly Pauli paramagnetic-like, although a non-negligible temperature-dependent component due to isolated Mo^{4+} spins is patent at low temperatures.

© 2006 Elsevier Inc. All rights reserved.

Keywords: Perovskite structure; Pauli paramagnetism

1. Introduction

Ternary oxides containing transition metals, for example the perovskite-type compounds ABO_3 (*B*: transition metals), are of great interest because of their electrical and magnetic properties. These properties are primarily related to the valence states of the transition metals involved. Twenty years ago, Goodenough established a scheme and gave a criterion for localized vs. collective *d*-electron behaviour in transition-metal oxides ABO_3 with perovskite structure [1,2]. According to this criterion, $AMoO_3$ (*A* = Ca, Sr, Ba) perovskites, nominally containing Mo^{4+} cations, have adequate electron transfer energies as to screen and cancel the electrostatic energy accompanied by the electron transfer. Thus, $AMoO_3$ can be classified into the superconducting possible materials. The low temperature electronic conductivities of these com-

pounds have been studied in the past: BaMoO₃ and SrMoO₃ are cubic perovskites showing metallic conductivity, and Pauli paramagnetism [3–5].

As for CaMoO₃, it was reported earlier as a monoclinic perovskite [6], but afterwards its stable form was proved to be orthorhombic [7,8]. CaMoO₃ was found also to show a metallic conduction and Pauli paramagnetism from room temperature to 77 K; these results indicated that the $4d^2$ electrons of Mo^{4+} are delocalized in CaMoO₃ [8]. Kamata et al. [9] reported the valence behaviour of alkaline earth molybdates for the various oxygen partial pressures and experimentally proved the presence of the oxygen stability ranges in these ternary oxides. These authors prepared a polycrystalline phase of CaMoO₄ by solid-state reaction from $CaCO_3$ and MoO_3. Ground and loosely pressed CaMoO₄ was suspended in a vertical furnace kept at $1200\,°C$ and at a desired oxygen partial pressure. The oxygen stability range of CaMoO₃ was investigated in O_2 partial pressures ranging from $\log P_{O_2} = -12.45$ to $\log P_{O_2} = -13.20$. The CaMoO₃ oxide prepared by this method, at $\log P_{O_2} = -12.62$, was found to have an

*Corresponding author. Fax: +34 313720623.

E-mail addresses: c.delacalle@icmm.csic.es (C. de la Calle), ja.alonso@icmm.csic.es (J.A. Alonso).

orthorhombic lattice ($a = 5.448$ Å, $b = 7.776$ Å, $c = 5.582$ Å). The narrow width of the oxygen stability range suggests the difficulty of obtaining $CaMoO_3$ by ordinary methods [6].

The aim of the present work is to describe a simple procedure to prepare stoichiometric $CaMoO_3$, by soft-chemistry procedures followed by a controlled reduction process, and to contribute to clarify the oxygen stoichiometry to crystal–structure relationship; we describe the characterisation from thermal analysis and neutron powder diffraction (NPD) data and we also report on the magnetic and electrical properties for this stoichiometric perovskite, for which we describe positive magnetoresistance at low temperatures.

2. Experimental

$CaMoO_3$ was obtained in powder form by a citrate technique. Stoichiometric amounts of analytical grade $CaCO_3$ and $(NH_4)_6Mo_7O_{24} \cdot 7H_2O$ were dissolved in citric acid. The solution was slowly evaporated, leading to an organic resin which was dried at $120\,^\circ C$ and slowly decomposed at temperatures up to $600\,^\circ C$ for 12 h. The sample was then heated at $800\,^\circ C$ for 2 h in order to eliminate all the organic materials, leading to a white precursor powder identified by X-ray diffraction (XRD) as $CaMoO_4$ with powellite structure. This precursor, very reactive, was then reduced at $900\,^\circ C$, H_2/N_2 (5%/95%) flow for 4 h.

The characterization by XRD was performed using a Bruker-axs D8 diffractometer (40 kV, 30 mA), controlled by a DIFFRACT^{plus} software, in Bragg-Brentano reflection geometry with Cu$K\alpha$ radiation ($\lambda = 1.5418$ Å). A secondary graphite monochromator allowed the complete removal of Cu$K\beta$ radiation. The data were obtained between 10° and 100° 2θ in steps of 0.05°. The slit system was selected to ensure that the X-ray beam was completely within the sample at all angles of 2θ.

Neutron powder diffraction (NPD) diagrams were collected at HRPT diffractometer [10] of the SINQ spallation source, at PSI, Villigen. The patterns were collected at room temperature with a wavelength of 1.494 Å. The high flux mode was used; the collection time was 3 h. An 8 mm dia. vanadium can was used. The refinement of the crystal structure was performed by the Rietveld method [11], using the FULLPROF refinement program [12]. A pseudo-Voigt function was chosen to generate the line shape of the diffraction peaks. The following parameters were refined in the final run: scale factor, background coefficients, zero-point error, pseudo-Voigt corrected for asymmetry parameters, positional coordinates, isotropic thermal factors and occupancy factors for oxygen atoms. The coherent scattering lengths for Ca, Mo and O were 4.700, 6.720 and 5.803 fm, respectively.

Thermal analysis was carried out in a Mettler TA3000 system equipped with a TC10 processor unit. Thermogravimetric profiles were obtained in a TG50 microbalance operating at 1 µg accuracy. About 45 mg of the sample was heated in an oxygen flow at $10\,^\circ C/min$ up to $900\,^\circ C$.

The magnetic susceptibility was measured with a commercial SQUID magnetometer on powdered samples, in the temperature range 5–400 K; transport measurements were performed by the conventional four-probe technique in a pellet sintered under the synthesis conditions. Magnetotransport measurements were carried out under magnetic fields up to 9 T in a PPMS system from Quantum Design.

3. Results and discussion

3.1. Thermal analysis

$CaMoO_3$ was obtained as a black polycrystalline powder. Fig. 1 shows the TG and DTG curves corresponding to the oxidation process of the sample in an oxygen flow. The weight gain starts above $300\,^\circ C$ and ends at around $600\,^\circ C$. The oxidation seems to be formed by only one process, with a DTG temperature peak at $520\,^\circ C$. The weight gain, of 9.24%, accounts for the incorporation of 1.06 (2) oxygen atoms per formula unit, corresponding to the total oxidation of Mo^{4+} to Mo^{6+}. The final product above $900\,^\circ C$ was identified by X-ray as $CaMoO_4$, powellite (PDF No.70212), which does not show a perovskite-like structure. Therefore, the composition of the initial material is $CaMoO_{2.94\,(2)}$, close to the expected full stoichiometry, $CaMoO_3$.

3.2. X-ray and neutron powder diffraction

The XRD pattern of $CaMoO_3$ compound is characteristic of a perovskite showing well-defined reflections corresponding to an orthorhombic superstructure, as displayed in Fig. 2. No impurity phases were detected either in XRD or NPD data. The crystal structure
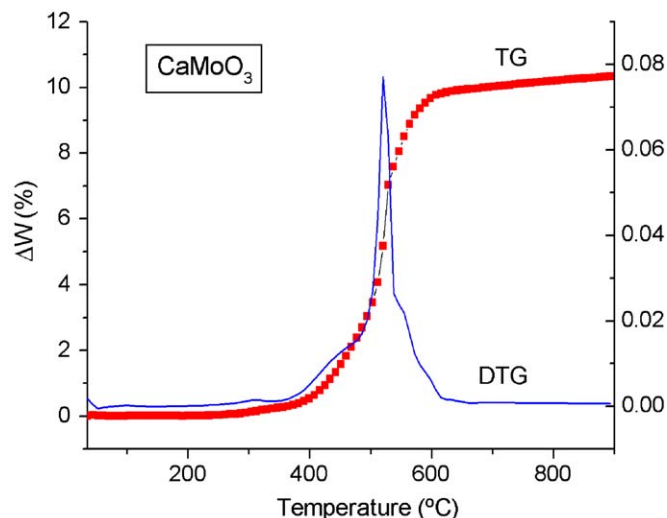

Fig. 1. Thermal analysis (TG and DTG) curves for $CaMoO_3$, in an oxygen flow.

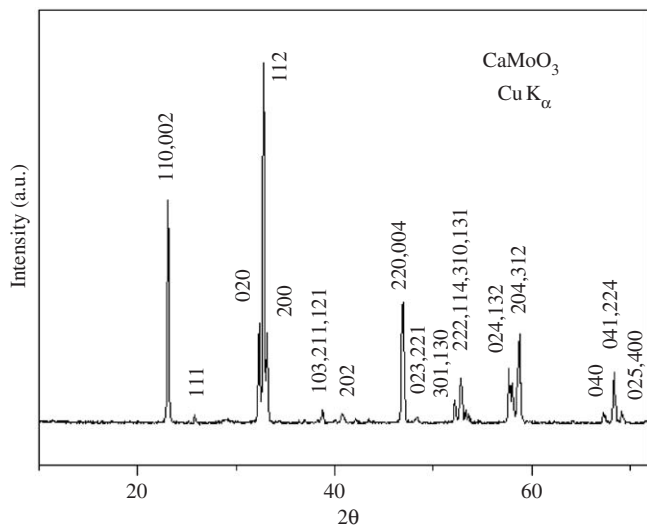Fig. 2. XRD pattern for $CaMoO_3$, indexed in an orthorhombic unit cell with $a = 5.4510\,(1)$ Å, $b = 5.5821\,(1)$ Å, $c = 7.7803\,(2)$ Å.

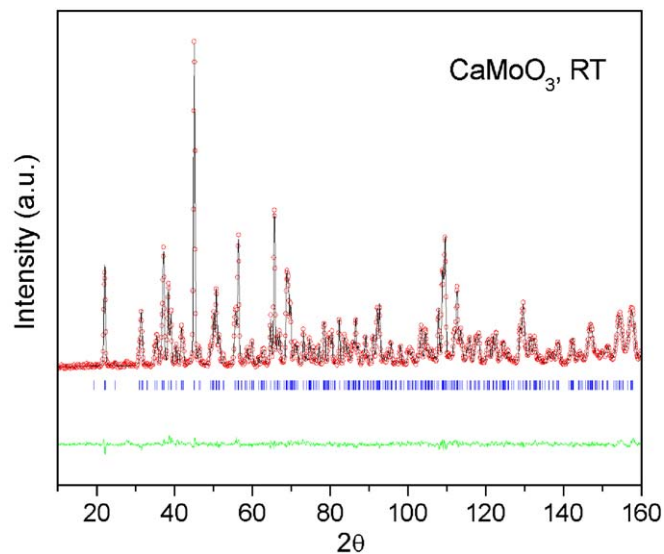

Fig. 3. Observed (circles), calculated (full line) and difference (bottom) NPD Rietveld profiles for orthorhombic $CaMoO_3$ at RT. The tick marks correspond to the allowed Bragg reflections.

refinement was performed from NPD data collected at room temperature (RT). The structure was defined in the orthorhombic space group *Pbnm* (No. 62), $Z = 4$, with the $GdFeO_3$-type structure [13]. The lattice parameters were $a = 5.4510(1)$ Å, $b = 5.5821(1)$ Å, $c = 7.7803(2)$ Å and $V = 236.74$ Å^3. Ca atoms were located at $4c$ positions, Mo atoms at $4b$ and oxygen atoms at $4c$ and $8d$ positions, respectively. The oxygen stoichiometry at O_1 and O_2 positions was checked by refining their occupancy factors; no oxygen vacancies were detected within the standard deviations. A good fit between the observed and the calculated profiles was obtained, as shown in Fig. 3. Table 1 lists the refined structural and thermal parameters, together with unit-cell parameters refined from NPD data at RT.

Table 2 includes the mean interatomic distances and some selected bond angles. The fit ($R_{Bragg} = 3\%$) obtained for this model allowed us to confirm that the tilting scheme of the MoO_6 octahedra corresponds to a $GdFeO_3$-like distortion of the perovskite. The structure of $CaMoO_3$ had previously been described as monoclinic [6]; the difficulty of preparing the stoichiometric material is probably the reason of this description. A NPD study was essential to investigate the structural features of this perovskite, neutrons being more sensitive to the oxygen positions. A view of the crystal structure of $CaMoO_3$ is shown in Fig. 4. Due to small size of Ca^{2+} cations, the MoO_6 octahedra are forced to tilt in order to optimize the Ca–O bond distances. The average tilting angle can be estimated as $\varphi = (180 - \theta)/2$ where $\theta = \langle Mo\text{–}O\text{–}Mo \rangle = 153.01°$, and $\varphi = 13.49°$.

As shown in Table 2, Ca–O distances, in the rather distorted CaO polyhedron, range from 2.37 to 3.13 Å; the effective coordination of Ca^{2+} cation can be considered as eightfold, only considering the bond-lengths below 2.71 Å, with an average $\langle Ca\text{–}O \rangle_{8\,short}$ value of 2.54 Å which compares well with that expected from ionic radii sums

Table 1
Structural parameters for $CaMoO_3$ refined in the orthorhombic *Pbnm* space group from NPD data at RT

Atom	Site	x	y	z	f_{occ}	B (Å)^2
Ca	$4c$	0.9895 (5)	0.0454 (3)	1/4	1.0	0.63 (3)
Mo	$4b$	1/2	0	0	1.0	0.17 (2)
O_1	$4c$	0.0810 (3)	0.4780 (3)	1/4	1.024 (8)	0.56 (4)
O_2	$8d$	0.7045 (2)	0.2931 (2)	0.0423 (2)	1.022 (6)	0.57 (2)

Lattice parameters: $a = 5.4510(1)$ Å, $b = 5.5821(1)$ Å, $c = 7.7803(2)$ Å and $V = 236.73(9)$ Å^3.
Reliability factors: $\chi^2 = 2.12$, $R_p\% = 3.09$, $R_{wp}\% = 4.38$ and $R_{Bragg}\% = 3.14$.

[14] of 2.52 Å for $^{VIII}Ca^{2+}$ (i.r.: 1.12 Å) and $^{VI}O^{2-}$ (i.r.: 1.40 Å). For the molybdenum-to-oxygen bonds the average distance of 2.005 (1) Å is in excellent agreement with that expected, of 2.050 Å for $^{VI}Mo^{4+}$ ions (r.i.:0.650 Å).

The phenomenological Brown's Bond-Valence Model (BVS) [15] relates the bond-length r_i and the valence s_i of a bond (for each central atom $v = \sum s_i$, $s_i = \exp[(r_0 - r_i)/0.37]$; $r_0 = 1.967$ and 1.907 for the Ca–O and Mo–O pairs [16]). Using this approach the calculated valences in the ionic limit, from RT data, are 1.82 (8) and 4.60 (8) for Ca and Mo cations, respectively. The valence of the Ca cations are slightly lower than $+2$; in compensation, the valence of Mo atoms is higher than the expected value of $+4$. This result suggests that Ca atoms are underbonded while Mo are overbonded in this structure; in others words Ca–O bonds are, in average, under tensile stress and Mo–O are under compressive stress, giving rise to a structure with a significant metastable character. The presence of structural stresses in the crystal structure can be quantified by means of the "Global Instability Index" [17], GII in Table 2, calculated as the root mean of the valence deviations for

Table 2
Main bond distances (Å) and selected angles (deg.) for orthorhombic $CaMoO_3$ determined from NPD data at RT

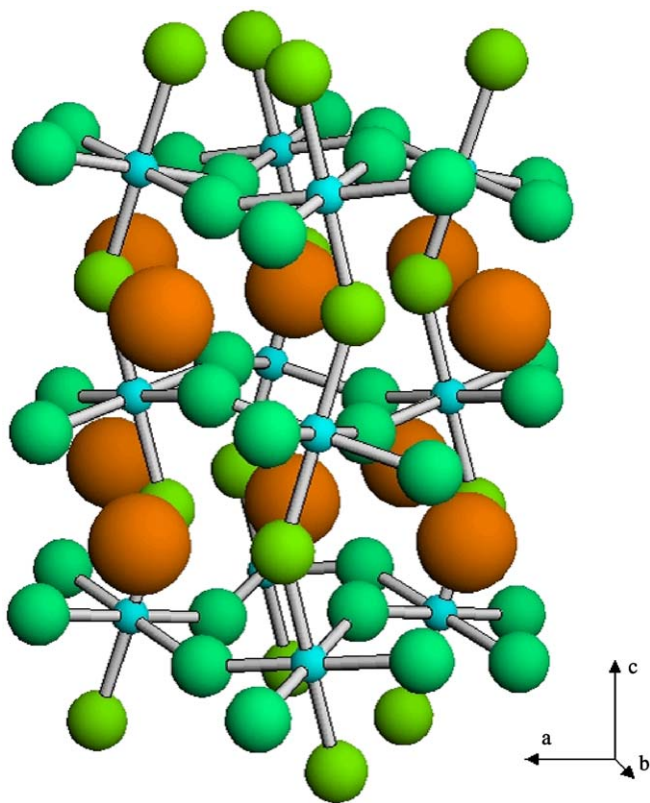| CaO_9 Polyhedra	
Ca–O_1	2.465 (3)
Ca–O_1[a]	3.133 (4)
Ca–O_1	2.371 (4)
Ca–O_2 ($\times 2$)	2.634 (2)
Ca–O_2 ($\times 2$)	2.391 (2)
Ca–O_2 ($\times 2$)	2.712 (2)
$\langle$Ca–O$\rangle_{(8\ short)}$	2.539 (1)
MoO_6 Octahedra	
Mo–O_1 ($\times 2$)	1.998 (1)
Mo–O_2 ($\times 2$)	2.007 (1)
Mo–O_2 ($\times 2$)	2.009 (1)
$\langle$Mo–O$\rangle$	2.005 (1)
Angles around O_1	
Mo–O_1–Mo	153.49 (5)
Angles around O_2	
Mo–O_2–Mo ($\times 2$)	152.52 (9)

[a]Long Ca–O distance.

Fig. 4. Schematic representation of the crystal structure of $CaMoO_3$ showing the tilting of the MoO_6 octahedra. Large spheres represent Ca atoms.

the $j = 1, \ldots, N$ atoms in the asymmetric unit according to $\mathrm{GII} = (\sum_j [\sum_i s_{ij} - V_j^2]/N)^{1/2}$, where $\sum_i s_{ij}$ is the valence of jth central atom. It is a measure of the extent to which the BVS rule is violated over the whole structure. GII is as high as 0.709; actually, crystal structures with GII higher than

0.1 are usually considered as seriously strained, which explains the difficulties found in the synthesis of this metastable oxide.

3.3. Magnetic and transport properties

The susceptibility and reciprocal susceptibility vs. temperature data are shown in Fig. 5a. Above 100 K, the almost temperature-independent observed susceptibility corresponds to the reported Pauli paramagnetism behaviour; below this temperature, the susceptibility shows significant temperature dependence. The total susceptibility $\chi(T)$ can be represented by

$$\chi(T) = \chi_{TIP} + \chi_{dia} + \chi_C(T),$$

with $\chi_C(T) = C/(T - \theta_{Weiss})$, where χ_{TIP}, χ_{dia} and $\chi_C(T)$ are the temperature-independent, diamagnetic and Curie–Weiss terms of the susceptibility. The susceptibility χ_{dia}, to which the ion cores contribute, is estimated to be -61×10^{-6} emu mol^{-1} Oe^{-1} for $CaMoO_3$. The fit to this equation gives a molar Pauli susceptibility, χ_{TIP}, of 2.48×10^{-4} emu mol^{-1} Oe^{-1}, $C = 2.81 \times 10^{-3}$ emu mol^{-1} Oe^{-1} K and $\theta_{Weiss} = -10$ K. For the value of C, the effective number of Bohr magnetons per Mo atom, p, equals $0.15\,\mu_B/Mo^{4+}$, which is strongly reduced with respect to expected spin-only moment of $2.83\,\mu_B$ for this
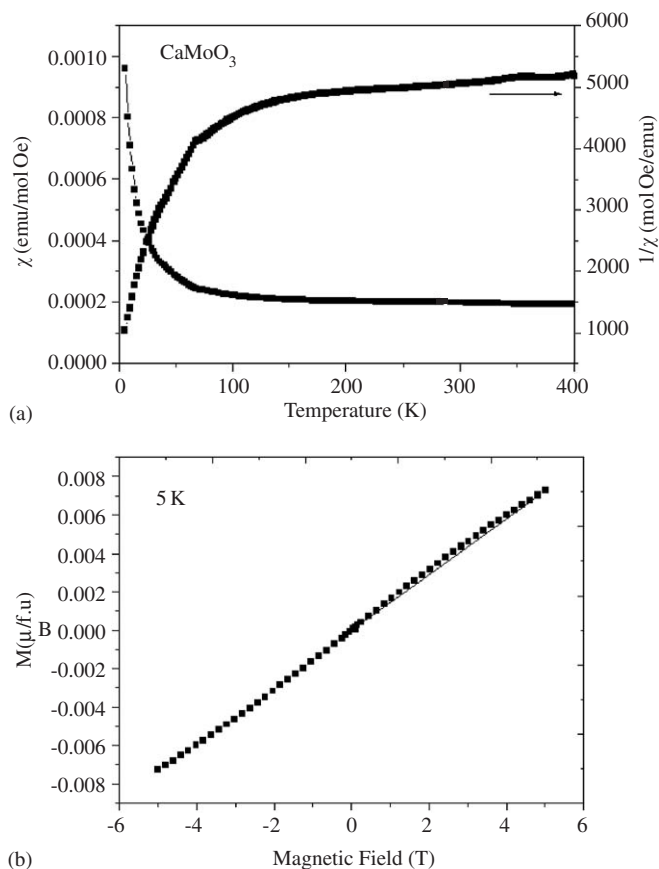

Fig. 5. (a) Temperature dependence of the magnetic susceptibility of $CaMoO_3$; (b) magnetization isotherm at 5 K.

sample. On the other hand, the calculated value for χ_{TIP} is larger than the Pauli susceptibility in mono-electronic classical metals (for instance, $\chi_m = 1.96 \times 10^{-4}$ emu mol^{-1} for metallic sodium). This enhanced value suggests a relatively strong correlation among $4d$ electrons in narrow π^* conduction bands of T_{2g} parentage. A similar behaviour has been observed in a number of transition metal oxides which are considered as correlated metallic systems. An example is CaVO$_3$ [18], with $\chi_{TIP} = 2.4 \times 10^{-4}$ emu mol^{-1} Oe^{-1} and $p = 0.14 \mu_B$ for V^{4+} ions.

The magnetization isotherm at 5 K (Fig. 5b) shows a virtually linear behaviour with the magnetic field, reaching negligible magnetization values of $0.007 \mu_B$/f.u. at the maximum field of 5 T, thus excluding the presence of weak-ferromagnetic interaction in this system.

The temperature dependence of the electrical resistivity is shown in Fig. 6a for $H = 0$ and an external applied magnetic field of $H = 8.5$ T. A metallic behaviour characterized by a positive slope is observed in all the temperature range; a resistivity of $\rho \approx 0.0085\,\Omega$ cm is observed at RT, and a residual resistivity at the lowest temperature of 20 K of 0.0035 Ω cm for $H = 0$. Previous reports of the resistivity vs. temperature [19] revealed that $AMoO_3$ ($A =$ Ba, Sr, Ca) are metallic in the temperature range from 300 K down to 2.5 K, and the residual resistivities at 4.2 K were determined to be $6.2 \times 10^{-4}\,\Omega$ cm (BaMoO$_3$), $1.4 \times 10^{-5}\,\Omega$ cm (SrMoO$_3$) and $1.8 \times 10^{-4}\,\Omega$ cm (CaMoO$_3$).

The resistivity curve recorded under an external field of $H = 8.5$ T shows very similar features, although a divergence from the $H = 0$ plot is observed below 150 K. We define the magnetoresistance ratio as MR$(H) = 100 \times [R(H) - R(0)]/R(0)$. Fig. 6b shows the evolution of MR vs. magnetic field in the $H = -9$ T to $+9$ T range at 5 K. A small positive magnetoresistance is observed, reaching a maximum value of 1.4% at 9 T. The magnetic field dependence of MR can be described as MR $\propto H^n$, and the value of the exponent n takes a value of 1.76 (8), intermediate between a linear and a parabolic behaviour of MR with the field. The positive magnetoresistance cannot obviously be understood by the spin-dependent scattering theory, which accounts for the decrease in resistance upon the application of an external magnetic field in a ferromagnetic material. The present kind of positive MR can be attributed to two different origins: (i) that found in normal metals is due to the curving of the carrier trajectory by a magnetic field leading to the observed increase in resistivity, and (ii) quantum interference effects, that take place in systems where the same electrons are responsible for both magnetic properties and electrical conduction. This quantum-interference magnetoresistance gives usually rise to a linear behaviour of MR vs. H [20]. On the other hand, a positive magnetoresistance with a MR $\propto H^n$ variation (n between 1 and 1.5) has been described in other systems like Fe$_x$C$_{1-x}$ composites [21]. The positive MR observed for CaMoO$_3$ perovskite at low-temperatures has probably the same origin to that observed

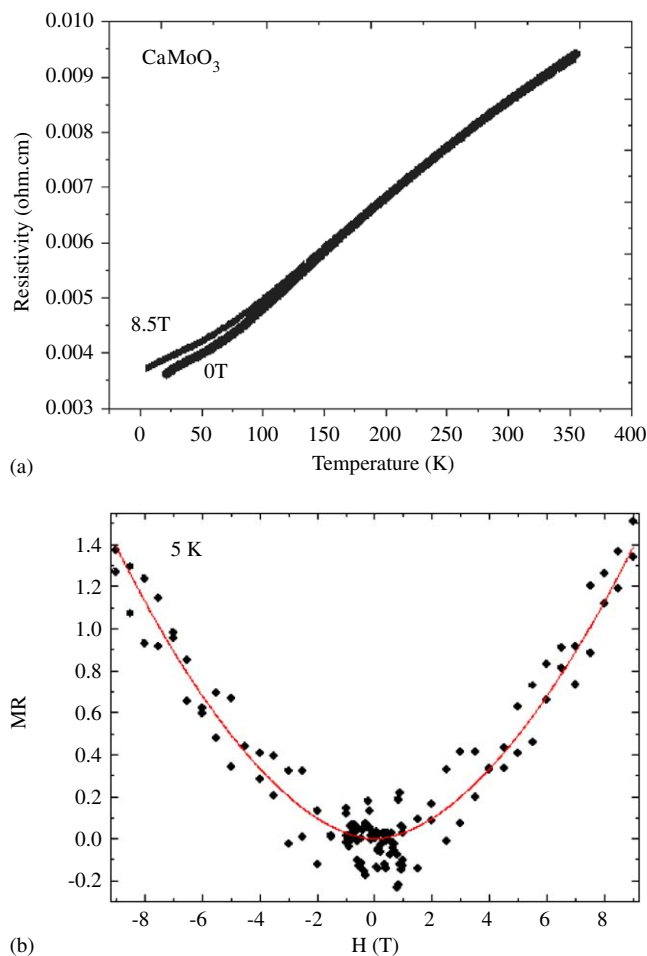Fig. 6. (a) Thermal variation of the electrical resistivity at $H = 0$ and 8.5 T; (b) magnetoresistance vs. magnetic field at 5 K. The solid line is a fit of MR to a AH^n function, with $A = 0.029$ (5), $n = 1.76$ (8).

in CaVO$_3$ [18] and in La$_{0.7}$Pb$_{0.3}$MnO$_3$ perovskite manganite between 4.2 and 50 K; this manganite additionally presents the more conventional and well-understood negative MR at higher temperatures [22].

4. Conclusion

We conclude that CaMoO$_3$ exhibits no significant deviations from the stoichiometric composition. No oxygen vacancies have been detected in the perovskite structure by refinement of the oxygen occupancy from neutron data. The Rietveld refinement also shows a full occupancy of the Ca and Mo positions. Both transport and magnetic measurements suggest that there is an important electronic delocalization in this system, giving rise to the observed metallic behaviour and a temperature-independent susceptibility term. The fairly high value of this term points to the existence of a relatively strong correlation among the $4d$ electron in the narrow π^*-like conduction bands. A positive magnetoresistance, approximately proportional to the square of the magnetic field, is observed at low temperatures, reaching a maximum value of 1.4% at

9 T and $T = 5\,K$, similar to that reported in other strongly correlated electron systems.

Acknowledgments

References

[1] J.B. Goodenough, J. Appl. Phys. 37 (1966) 1415.

[2] J.B. Goodenough, J.M. Longo, Landolt-Borstein Zahlenwerte und Funktionen, New Series BdIII/4a (1970) 255.

[3] L.H. Brixner, J. Inorg. Nucl. Chem. 14 (1960) 225.

[4] G.H. Bouchard, M.J. Sienko, Inorg. Chem. 7 (1968) 441.

[5] S. Hayashi, R. Aoki, T. Nakamura, Mater. Res. Bull. 14 (1979) 409.

[6] W.H. McCarroll, R. Ward, L. Katz, J. Am. Chem. Soc. 78 (1956) 2909.

[7] W.H. McCarroll, L. Katz, R. Ward, J. Am. Chem. Soc. 79 (1957) 5410.

[8] K. Kamata, T. Nakamura, T. Sata, Chem. Lett. 1 (1975) 81.

[9] K. Kamata, T. Nakamura, T. Sata, Mater. Res. Bull. 10 (1975) 373.

[10] P. Fischer, G. Frey, M. Koch, M. Koennecke, V. Pomjakushin, J. Schefer, R. Thut, N. Schlumpf, R. Buerge, U. Greuter, S. Bondt, E. Berruyer, Physica B 46 (2000) 276.

[11] H.M. Rietveld, J.Appl. Crystallogr. 2 (1969) 65.

[12] J. Rodriguez-Carvajal, Physica B 192 (1993) 55.

[13] S. Geller, J. Chem. Phys. 24 (1956) 1236.

[14] R.D. Shannon, Acta Crystallogr. A 32 (1976) 751.

[15] I.D. Brown, in: M. O'Keefe, A. Navrotsky (Eds.), Structure and Bonding in Crystals, vol. 2, Academic Press, New York, 1981, pp. 1–30.

[16] N.E. Brese, M. O'Keefe, Acta Crystallogr. B 47 (1991) 192.

[17] I.D. Brown, Z. Kristallogr. 199 (1992) 255.

[18] H. Falcon, J.A. Alonso, M.T. Casais, M.J. Martinez-Lope, J. Sanchez Benitez, J. Solid State Chem. 177 (2004) 3099.

[19] S. Hayashi, R. Auki, Mater. Res. Bull. 14 (1979) 409.

[20] A.A. Abrikosov, J. Phys. A: Math. Gen. 36 (2003) 9119.

[21] Q.Z. Xue, X. Zhang, D.D. Zhu, J. Magn. Magn. Mater. 270 (2004) 397.

[22] P. Chen, D.Y. Xing, Y.W. Du, Phys. Rev. B 64 (2001) 104402.